Rigaku

X-ray Diffraction & Elemental Analysis

橋 THE BRIDGE

MATERIALS ANALYSIS eNEWSLETTER

JUNE 2014, ISSUE 12

Welcome

One of my favorite wildlife photos is of a gorilla crossing a river and using a stick as a measuring device to, I assume, prevent him from drowning. It shows the natural tendency to measure things and that it is probably a primitive behavior that we learned from our primate ancestors. In a sense, the discovery of X-rays was just the discovery of another measuring device, and mankind continues to fine tune this device and find new things to measure. Our X-ray measurement are not always a life and death measurement, but sometimes they are — we all feel more confortable knowing that cement and steel used to build a bridge were properly qualified by X-ray analysis, and the world would not be as a safe a place if our pharmaceuticals were not held to high standards to ensure that the proper polymorph is being delivered.

In our own way, each of us helps the gorilla from drowning in the river.

Enjoy the newsletter.

BRIDGE 橋

A bridge is often used to symbolize a connection or link between two places, and thus we felt The Bridge would be the perfect name for our eNewsletter, as we hope that it will act as a vehicle for the transmission of ideas and information between Rigaku and interested readers around the world.

And a bridge is a two-way structure, a concept that we will keep in mind as we not only provide information about Rigaku, but also report on interesting research and the associated laboratories around the world, publish technical book reviews that might help our readers in their work, and highlight general news topics that are of interest to many people involved in materials analysis.

Photo by Paul Swepston

Featured Rigaku Journal Article

Crystallite size distribution analysis software "CSDA"

Application & Software Development, Rigaku Corporation

"CSDA" is a unique method to derive crystallite size and its "distribution" profile from a single diffraction line recorded by Bragg-Brentano configuration. The sample type can be in powder form, thin film or bulk forms. The conventional method, e.g. Scherrer method, assumes that there is no distribution in terms of the crystallite size but this CSDA method takes it into account. The CSDA functionality is now integrated into the PDXL software basic package.

Click here for full article

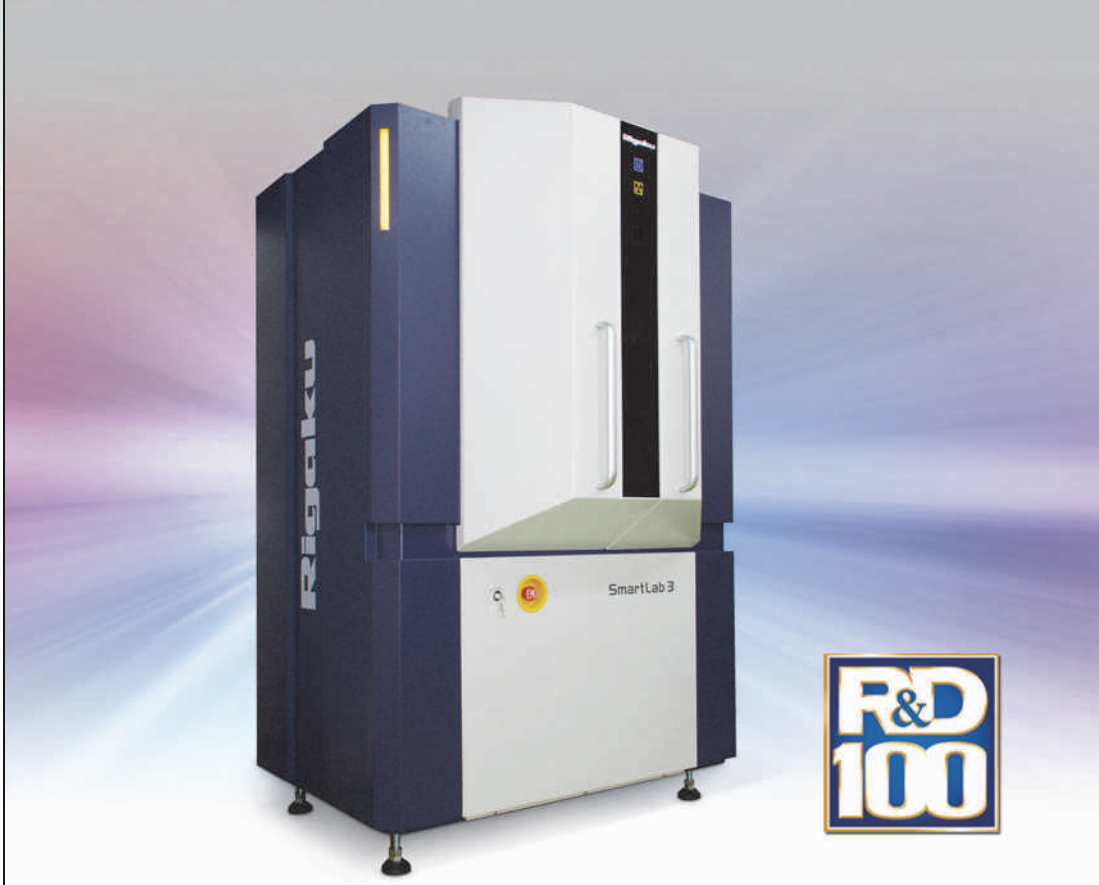

Introducing SmartLab® 3 diffractometer, the latest member of the SmartLab family

The latest SmartLab model, the SmartLab 3 system, offers continued refinement of the original ease-of-use features awarded the R&D 100 Award in 2006: automatic alignment, component recognition, cross beam optics and a five axis goniometer.

Automatic alignment controls and optimizes the positions of all system components. The complete optical path, comprised of X-ray source, optics, sample stage and detector, is automatically aligned in fifteen minutes.

Award winning guidance software recognizes installed components and seamlessly integrates them into data collection and data analysis methods.

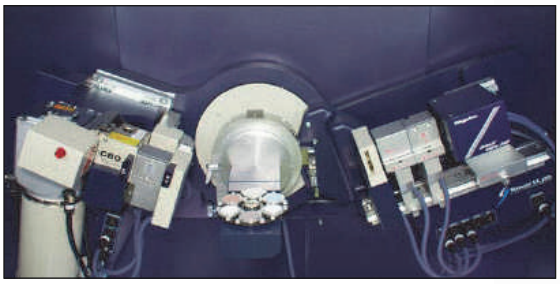

SmartLab 3 diffractometer in powder configuration

Cross beam optics offers permanently mounted, permanently aligned and user selectable optical geometries for various diffraction experiments.

As an example, you can choose a Bragg-Brentano and parallel beam combination for measurements of both powders and thin films without the need for instrument reconfiguration.

You could also choose a Bragg-Brentano and focusing transmission combination to measure organic materials in both transmission and reflection modes.

The fifth, or in-plane, axis of the SmartLab 3 diffractometer allows the measurement of structures that are in the surface plane of the sample. This allows the measurement of extremely thin films and depth profiling in coatings.

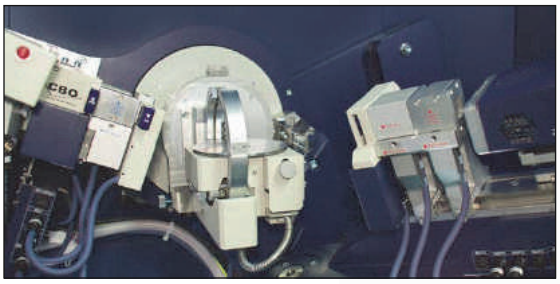

The SmartLab 3 system's 5th axis allows in-plane scanning of thin film materials

The newest additions to the SmartLab 3 system is the HyPix-400 0, 1, and 2-D detection system. This hybrid pixel array detector, the type currently being used at most synchrotron beamlines, offers the highest resolution and count rates available today. They are fully manufactured and integrated into the SmartLab 3 system by Rigaku and, as such, offer the superior ease of use pioneered by Rigaku in the original SmartLab model. The SmartLab 3 diffractometer configured with HyPix-400 detector operates in 0, 1, and 2-D modes without the need to exchange a detector.

HyPix-400 hybrid pixel array detector

D/teX Ultra 250 Si strip detector

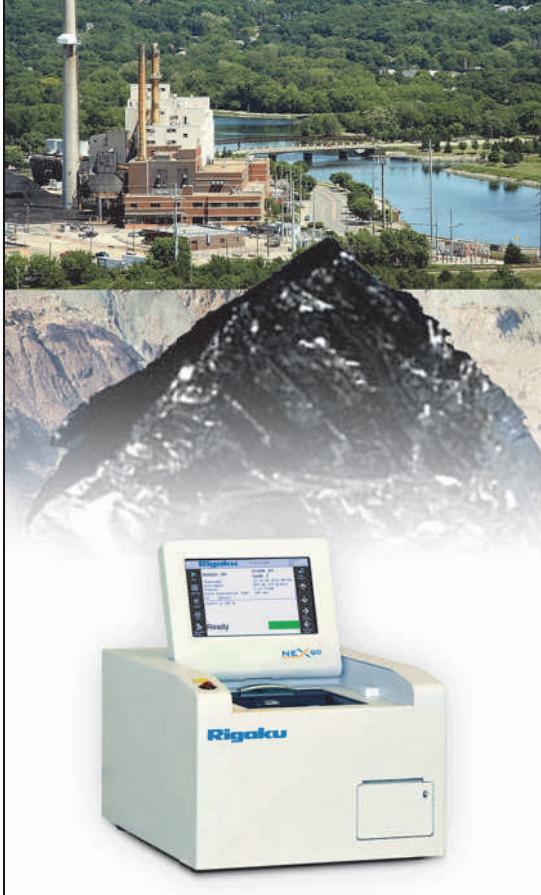

Featured EDXRF Application Note

Predicting % Ash Content in Coal

Applied Rigaku Technologies

Ash consists of the metal oxides and heavier elements that remain after burning removes the organic, gaseous and volatile components. Coal quality and pricing in part depends on the ash content of the coal, and so predicting ash in coal before burning is important in many areas of the industry. EDXRF offers a fast and simple low cost method of predicting the % ash content in coal before it is burned.

Click here to see full application note

An amazingly versatile instrument for powder and single crystal analysis

The RAPID II is arguably the most versatile X-ray area detector in the history of materials analysis. In production for well over a decade and continuously improved during that time period, the success of the RAPID II is a testament to the suitability of imaging plate technology for measuring diffraction patterns and diffuse scattering from a wide range of materials.

Click here for more information on Rigaku's D/MAX RAPID II

Lab in the Spotlight

Dr. Jens Najorka at the X-ray Lab in the Science Facilities Department, Imaging and Analysis Center

The Natural History Museum, London

A D/MAX RAPID II was installed as a powder XRD microdiffraction system by Dr. Jens Najorka at the X-ray lab in the Science Facilities Department, Imaging and Analysis center in the Natural History Museum, London (NHM).

X-ray Lab manager Dr. Jens Najorka is very impressed by the versatility of the D/MAX RAPID II, which is capable of analyzing powdered materials as well as single crystals.

The NHM was established in 1891 as a part of the British Museum. It is one of the biggest tourist attractions in London, with over 5 million visitors last year. The museum houses world-renowned collections, such as the mineral collection with over 350,000 specimens. We can find their most valuable collections of fine gems,

The famous Mineral Gallery including the Vault

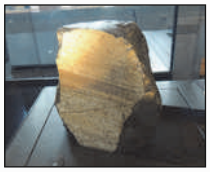

Meteorite from Mars and watermelon tourmaline

crystals and the Nakhla meteorite in their Vault gallery.

The NHM not only attracts a large number of visitors, it is also one of the world's leading authorities and research institutes in natural history. Its X-ray laboratory operates as an interdepartmental resource for both museum scientists and visiting researchers from around the world, and additionally contributes to income generation and consultancy from several of the museum's consultancy sectors.

The characterization of unknown minerals plays a major role for the X-ray laboratory at NHM. Dr. Jens Najorka and his co-workers use powder and single crystal XRD for research on an extremely wide range of materials, such as rocks, ores, sediments, meteorites, peats and soils, biominerals and manufactured materials. A remarkable number of unknown minerals have been studied in the lab.

As time goes by, samples are getting more challenging. Often, only a very small amount (a few milligrams) of a material or one single crystal fragment is available, or the material can only be analyzed on a tiny spot in a polished section. Versatility and combination of measurement techniques becomes essential in order to provide the best possible sample characterization.

The D/MAX RAPID II is a perfect addition to the NHM lab, as it comes with a number of stages for reflection and transmission geometries for both single crystal and powder samples. The unique large area detector is clearly beneficial for characterizing challenging micro-samples such as micrometeorites, mini-dust samples from airborne particulates or tiny calcified skeletons of marine species. The fact that the stage is capable of quasi-Gandolfi movements will be used to study single crystals, or crystal fragments for identification of potentially new minerals.

The X-ray lab at NHM has a tradition of quantification of mineral proportions by

using external standards from its huge mineral collection. Often, it is the only way to quantify samples containing clays or poorly crystallized sheet silicates where crystal structure models are not available and the Rietveld technique is not applicable. Using the large area detector of the D/MAX RAPID II is an advantage here as preferred orientation effects can be minimized by integrating data over large parts of the collected Debye rings (in order to maximize averaging and integrated counts), which is an impossible task for standard point or linear detectors.

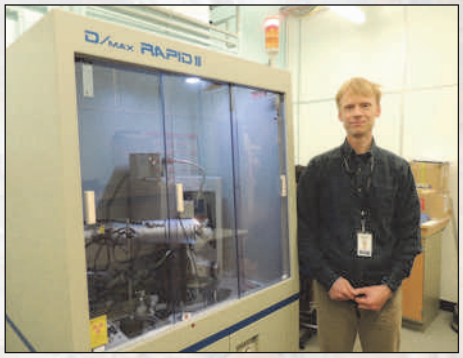

Dr. Jens Najorka with D/MAX RAPID II

Dr. Jens Najorka and his co-workers expect to use the unique flexibility of the D/MAX RAPID in a number of projects, that involve research on new minerals, modal mineralogy of meteorites, provenance tracing of dust sources and impacts of climate-change -induced ocean acidification.

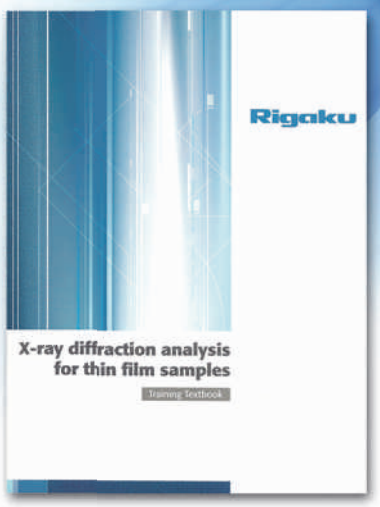

Thin Film Training Textbook

Overview of the principles of X-ray reflectivity (Part 6)

This month we continue a chapter on the principles of X-ray reflectivity by focusing on the analysis methods. Reflectivity can be analyzed by the three following methods:

1. Method giving film thickness based on the incident angle dependence of the oscillation period.
2. Method giving film thickness via the **Fourier transformation**.
3. Method giving film thickness, density, and surface or interface roughness by fitting.

Click here for Part 6

Conferences and Workshops

Join Rigaku at future meetings

Rigaku is entering the busy time of tradeshows, exhibitions, and training classes. Shown above are crystallographers who attended the ACA meeting in Albuquerque, USA recently and participated in Rigaku's Lunch and Learn program.

Rigaku will be sponsoring, attending or exhibiting at the following conferences and trade shows:

EPDIC14
Aarhus, Denmark
June 15 – 18

Northwest Crystallography Workshop
Corvallis, Oegon, USA
June 20 – 22

The Korea Conference
Seoul, South Korea
June 23 – 25

See the complete list

Material Analysis in the News

June 2, 2014. Specimen-mount procedure can affect Bragg peak positions and intensities in an X-ray powder-diffraction experiment of pharmaceutical APIs, especially for compounds that exhibit preferred orientation in powder diffraction. The authors examined several types of specimen holders to aid understanding of the effects of preferred orientation.

June 2, 2014. A new book, *Practical Raman spectroscopy: an introduction*, presents Raman scattering in a way that is understandable to non-specialists who may never have studied physical sciences at undergraduate level. The author, Peter Vandenabeele, is professor of archaeology at Ghent University.

June 10, 2014. Liquid explosives detectors, based on a variety of technologies, are entering service at airports. Restrictions on carrying liquids in your hand luggage could soon be a thing of the past. Manufacturers of liquid explosive detectors tend to concentrate on either X-rays or wavelengths closer to the spectrum of visible light.

June 10, 2014. Hamilton Kerr Institute paintings conservator Christine Slottvedd Kimbriel discussed how a variety of materials analysis techniques are used to confirm the authenticity of a self-portrait by Rembrandt..

June 11, 2014. Queensland Bauxite (ASX:QBL) shares have been placed in a trading halt at the request of the company by the Australian Stock Exchange in relation to material results on its bauxite project in north Queensland. The company had revealed in November last year that drilling and XRF testing had resulted in the discovery of a bauxite field at its South Johnston project.

June 11, 2014. A report by consultant Öko Institut has reviewed 21 substances that could be prioritised for addition to the Directive on the restriction of the use of certain hazardous substances (RoHS2) in electrical and electronic equipment (EEE). The report, contracted by the European Commission, says that the substances should be prioritised based on their quantities and on the possible differences in use by EU and non-EU manufacturers.

June 11, 2014. Using a state-of-the-art microscope and new methods in image processing, a multi-institutional team of researchers has devised an inventive way to measure the positions of single atomic sites in materials more precisely than ever before. Paul Voyles and his team uses a state-of-the-art scanning transmission electron microscope (STEM) at UW-Madison to gather experimental data, measuring atomic structures at the picometer scale.

June 13, 2014. During the recent decades enormous efforts have been made to develop efficient X-ray optics, utilizing different physical principles. The multilayer Laue lenses concept, used at the Fraunhofer IWS and TU Dresden, represents a very promising approach to efficiently focusing hard X-rays.

June 16, 2014. Earth's most abundant mineral lies deep in the planet's interior. A sample was recently discovered inside a 4.5-billion-year-old meteorite. The official name, bridgmanite, was approved for the rock formerly known by its chemical components — silicate-perovskite. The magnesium-silicate mineral was named after Percy Bridgman, a 1946 Nobel Prize-winning physicist.

Scientific Book Review

X-ray Line Profile Analysis in Material Science
By Jenö Gubicza

Engineering Science Reference, Hershey, 2014, 343 pages.
ISBN 978-1-4666-5852-3

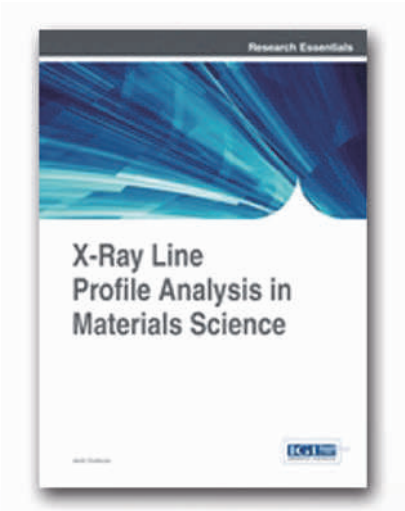

The author set out to provide a survey of the field of X-ray line profile analysis (XLPA) for the materials sciences. The book covers basic and advanced XLPA, and attempts to fill in the gaps in the current literature. From my perspective, the author has done a reasonably good job. The book is divided into nine chapters. Each provides an introduction and a conclusion, which covers the content of the chapter nicely. Each chapter also has its own list of references, and a compilation of references is provided at the end.

Chapter 1 discusses the fundamentals of kinematical X-ray scattering, including derivation of scattering intensity, the reciprocal lattice, the Ewald construction and Bragg's law. The second chapter covers broadening of diffraction profiles as a result of crystallite size and ends with analyses of spherical and anisotropic crystallites. Chapter 3 looks at the effects of strain on peak broadening. The results for dislocations for cubic, hexagonal and orthorhombic systems are also discussed in this chapter, and three practical examples are given. Chapter 4 covers broadening from planar faults, while Chapter 5 looks at the effects of chemical heterogeneities.

Chapter 6 reviews the methods for the evaluation of profiles, including the classical and modified Warren-Averbach methods, multiple whole profile fitting, classical and modified Williamson-Hall methods, variance methods, whole powder pattern fitting and modeling and, finally, convolutional multiple whole profile fitting.

Chapter 7 discusses profile evaluation for thin films, and Chapter 8 does the same for single crystals. Chapter 9 reviews the importance of the instrument function, since it impacts the line shape, and then surveys a number of practical examples.

The editors should have taken a little more time to ensure that the English is correctly written. There are a few places where a reader might break stride to go back and double check what they have just read. I did not find any errors in the equations, but there are a few places where the font is so small that it is barely legible.

Joseph D. Ferrara, Ph.D.
Chief Science Officer, Rigaku

Recent Scientific Papers of Interest

Analysis of spherical polyelectrolyte brushes by small angle X-ray scattering. Yu, Xuan-ji; Wang, Wei-hua; Li, Li; Guo, Xu-hong; Zhou, Zhi-min; Wang, Fu-chen. Chinese Journal of Polymer Science (Springer Science & Business Media B.V.). Jun2014, Vol. 32 Issue 6, p778-785. 8p. DOI: 10.1007/s10118-014-1456-3.

X-ray diffraction study of the $YbM^{II}_3Fe_5O_{12}$ (M^{II} = Mg, Ca, Sr) ferrites. Mustafin, E.; Mataev, M.; Kasenov, R.; Pudov, A.; Kaikenov, D.; Bogzhanova, Zh. Inorganic Materials. Jun2014, Vol. 50 Issue 6, p622-624. 3p. DOI: 10.1134/S0020168514060132.

ELEMENTAL COMPOSITION OF AIR PARTICULATE (PM10) IN SOFIA BY EDXRF TECHNIQUES. Veleva, Blagorodka; Hristova, Elena; Nikolova, Emilia; Kolarova, Maria; Valcheva, Ralica. Journal of Chemical Technology & Metallurgy. 2014, Vol. 49 Issue 2, p163-169. 7p. (PDF)

Characterization of metal hydrides by in-situ XRD. Bösenberg, Ulrike; Pistidda, Claudio; Tolkiehn, Martin; Busch, Nina; Saldan, Ivan; Suarez-Alcantara, Karina; Arendarska, Anna; Klassen, Thomas; Dornheim, Martin. International Journal of Hydrogen Energy. Jun2014, Vol. 39 Issue 18, p9899-9903. 5p. DOI: 10.1016/j.ijhydene.2014.02.068.

Experimental and theoretical FT-IR, Raman and XRD study of 2-acetyl-5-chlorothiophene. Chidan Kumar, Chandraju Sadolalu; Parlak, Cemal; Fun, Hoong-Kun; Tursun, Mahir; Keşan, Gürkan; Chandraju, Siddegowda; Quah, Ching Kheng. Spectrochimica Acta Part A: Molecular & Biomolecular Spectroscopy. Jun2014, Vol. 127, p67-73. 7p. DOI: 10.1016/j.saa.2014.02.033.

Competition behaviour of metal uptake in cementitious systems: An XRD and EXAFS investigation of Nd- and Zn-loaded 11Å tobermorite. Vespa, M.; Dähn, R.; Wieland, E. Physics & Chemistry of the Earth - Parts A/B/C. Jun2014, Vol. 70-71, p32-38. 7p. DOI: 10.1016/j.pce.2014.01.001.

Thermal behavior of cashew gum by simultaneous TG/DTG/DSC-FT-IR and EDXRF. Mothé, Cheila; Freitas, Jaqueline. Journal of Thermal Analysis & Calorimetry. Jun2014, Vol. 116 Issue 3, p1509-1514. 6p. DOI: 10.1007/s10973-014-3788-1.

Holographic Interferometry (HI), Infrared Vision and X-Ray Fluorescence (XRF) spectroscopy for the assessment of painted wooden statues: a new integrated approach. Sfarra, Stefano; Ibarra-Castanedo, Clemente; Ridolfi, Stefano; Cerichelli, Giorgio; Ambrosini, Dario; Paoletti, Domenica; Maldague, Xavier. Applied Physics A: Materials Science & Processing. Jun2014, Vol. 115 Issue 3, p1041-1056. 16p. DOI: 10.1007/s00339-013-7939-1.

***In situ* XAS and XRF study of nanoparticle nucleation during O_3-based Pt deposition.** Filez, Matthias; Poelman, Hilde; Ramachandran, Ranjith K.; Dendooven, Jolien; Devloo-Casier, Kilian; Fonda, Emiliano; Detavernier, Christophe; Marin, Guy B. Catalysis Today. Jun2014, Vol. 229, p2-13. 12p. DOI: 10.1016/j.cattod.2014.01.011.

Sample Preparation and X-Ray Fluorescence Analysis of Sulfide Ores. Ling, Ming-Xing; Liu, Ying; Zhang, Hong; Sun, Weidong. Analytical Letters. Jun2014, Vol. 47 Issue 9, p1598-1605. 8p. DOI: 10.1080/00032719.2013.876542.

X-ray fluorescence analysis with micro glass beads using milligram-scale siliceous samples for archeology and geochemistry. Ichikawa, Shintaro; Nakamura, Toshihiro. Spectrochimica Acta Part B. Jun2014, Vol. 96, p40-50. 11p. DOI: 10.1016/j.sab.2014.04.002.

X-ray absorption, X-ray diffraction and electron microscopy study of spent cobalt based catalyst in semi-commercial scale Fischer–Tropsch synthesis. Tsakoumis, Nikolaos E.; Dehghan-Niri, Roya; Rønning, Magnus; Walmsley, John C.; Borg, Øyvind; Rytter, Erling; Holmen, Anders. Applied Catalysis A: General. Jun2014, Vol. 479, p59-69. 11p. DOI: 10.1016/j.apcata.2014.03.035.

High pressure and high temperature *in situ* X-ray diffraction studies in the Paris-Edinburgh cell using a laboratory X-ray source. Toulemonde, Pierre; Goujon, Céline; Laversenne, Laetitia; Bordet, Pierre; Bruyère, Rémy; Legendre, Murielle; Leynaud, Olivier; Prat, Alain; Mezouar, Mohamed. High Pressure Research. Jun2014, Vol. 34 Issue 2, p167-175. 9p. DOI: 10.1080/08957959.2013.873425.

***In-situ* X-ray diffraction activation study on an Fe/TiO_2 pre-catalyst.** Rayner, Matthew K.; Billing, David G.; Coville, Neil J. Acta Crystallographica: Section B, Structural Science, Crystal Engineering & Materials. Jun2014, Vol. 70 Issue 3, p498-509. 12p. DOI: 10.1107/S2052520614011238.

Three-dimensional X-ray diffraction in the diamond anvil cell: application to stishovite. Nisr, Carole; Ribárik, Gábor; Ungár, Tamás; Vaughan, Gavin B.M.; Merkel, Sébastien. High Pressure Research. Jun2014, Vol. 34 Issue 2, p158-166. 9p. DOI: 10.1080/08957959.2014.885021.

X-ray micro-diffraction studies of heterogeneous interfaces between cementitious materials and geological formations. Dähn, R.; Popov, D.; Schaub, Ph.; Pattison, P.; Grolimund, D.; Mäder, U.; Jenni, A.; Wieland, E. Physics & Chemistry of the Earth - Parts A/B/C. Jun2014, Vol. 70-71, p96-103. 8p. DOI: 10.1016/j.pce.2013.10.010.

Local atomic structure of chromium bearing precipitates in chromia doped uranium dioxide investigated by combined micro-beam X-ray diffraction and absorption spectroscopy. Kuri, G.; Mieszczynski, C.; Martin, M.; Bertsch, J.; Borca, C.N.; Delafoy, Ch. Journal of Nuclear Materials. Jun2014, Vol. 449 Issue 1-3, p158-167. 10p. DOI: 10.1016/j.jnucmat.2014.03.017.

***In situ* synchrotron X-ray diffraction study on the dehydrogenation behavior of $LiAlH_4$–MgH_2 composites.** Hsu, Wei-Che; Yang, Cheng-Hsien; Tan, Chia-Yen; Tsai, Wen-Ta. Journal of Alloys & Compounds. Jun2014, Vol. 599, p164-169. 6p. DOI: 10.1016/j.jallcom.2014.02.064.

***In-situ* high pressure X-ray diffraction studies of orthoferrite $SmFeO_3$.** Na-Na Li; Yan Li; Hui Li; Rui-Lian Tang; Yong-Sheng Zhao; Dan-Dan Han; Yan-Mei Ma; Qi-Liang Cui; Pin-Wen Zhu; Xin Wang. Chinese Physics B. Jun2014, Vol. 23 Issue 6, p1-1. 1p. DOI: 10.1088/1674-1056/23/6/069101.

Depletion-induced sphere-cylinder transition in $C_{12}E_5$ microemulsion: a small-angle X-ray scattering study. Amirkhani, Masoud; Sharifi, Soheil; Funari, Sérgio S.; Marti, Othmar. Molecular Physics. Jun2014, Vol. 112 Issue 12, p1702-1709. 8p. DOI: 10.1080/00268976.2013.860243.

The Adventures of Captain Nano

THE GOOD, THE BAD & THE DOGGED — Why they call him Captain Nano.

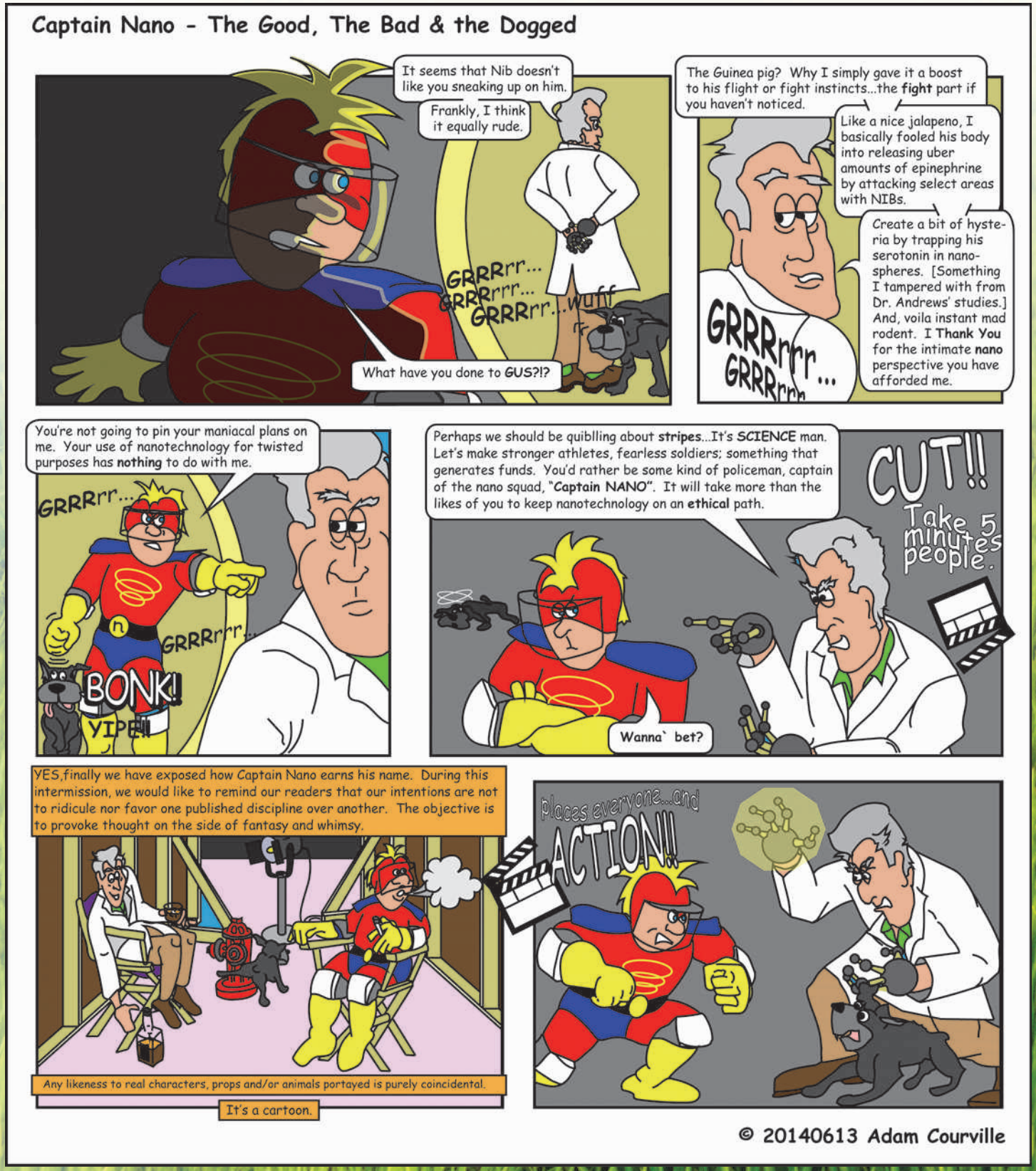

EDXRF Application Note

Predicting % Ash Content in Coal

#1378

SCOPE

Measurement of predicted ash content in unburned coal is demonstrated here.

BACKGROUND

Ash consists of the metal oxides and heavier elements that remain after burning removes the organic, gaseous and volatile components. Coal quality and pricing in part depends on the ash content of the coal, and so predicting ash in coal before burning is important in many areas of the industry. EDXRF offers a fast and simple low cost method of predicting the % ash content in coal before it is burned.

INSTRUMENTATION

Model:	Rigaku NEX QC
X-ray tube:	4 W Ag-anode
Detector:	Semiconductor
Sample Type:	Coal
Film:	Mylar
Analysis Time:	130 sec
Environment:	Air
Sample Prep:	Grinder or mill
	Rigaku Manual Sample Press
Optional:	Autosampler

Applied Rigaku Technologies, Inc. • 9825 Spectrum Drive, Bldg. 4, Suite 475 • Austin, TX 78717 USA
www.RigakuEDXRF.com • info@RigakuEDXRF.com • (+1) 512-225-1796

SAMPLE PREPARATION & PRESENTATION

Sample Grinding

The site field samples used to show the data here were ground to grain size 18-60 mesh (1mm – 250um particle size). Performance can be enhanced using grinding to a medium powder approximately 100-200 mesh (150-75um particle size).

Quick and Easy Sample Compaction

For best ash measurements, consistent sample height is important. Samples first are ground to a homogeneous powder. To achieve consistent sample height weigh 5.0g of sample into a sample cup and compact to 250 inch-pounds torque using Manual Sample Press.

Manual Sample Press

CALIBRATION

To create calibration standards, two homogeneous splits are taken from a homogeneous bulk sample. One split is ashed to determine the % ash content. This % ash number is then assigned to the unburned split as an assay for use as an XRF calibration standard. Separate calibrations may be required for each different coal type of interest, for example separate calibrations for lignite and bituminous coal.

To demonstrate use at a coal facility, eight calibration standards were collected from the site and were used to build an empirical calibration. % Ash measurements were automatically optimized using matrix corrections for iron, sulfur and silicon.

% Ash	Std Error of Est: 0.4663 Correlation: 0.998221	
Standard I.D.	Assay Value	Measured Value
1	25.3	25.6
2	19.3	19.3
3	18.2	18.6
4	24.2	23.9
5	20.4	20.1
6	29.8	29.7
7	17.9	17.8
8	34.2	34.3

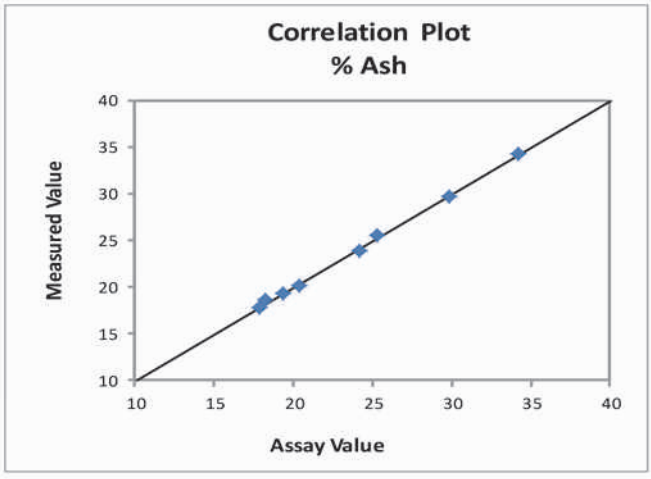

Applied Rigaku Technologies, Inc. • 9825 Spectrum Drive, Bldg. 4, Suite 475 • Austin, TX 78717 USA
www.RigakuEDXRF.com • info@RigakuEDXRF.com • (+1) 512-225-1796

REPEATABILITY (Precision)

To demonstrate repeatability, four calibration standards were selected that spread across the % ash concentration range. Each was measured in 10 repeat analyses using an analysis time of 130 sec per sample without moving the sample between measurements to determine and average value for precision. If desired, repeatability can be enhanced by using consistent 100-200 mesh grinding and longer measurement times.

Sample	% Ash Assay Value	% Ash Calibration Value	% Ash Average Value	Std Dev	% Relative Dev
7	17.9	17.8	18.0	0.3	1.7
4	24.2	23.9	23.7	0.3	1.3
6	29.8	29.7	29.7	0.3	1.0
8	34.2	34.3	34.4	0.3	0.9

CONCLUSION

The NEX QC offers the lab analyst or field operator at the site a simple and fast tool for predicting % ash content in coal. The versatility of the NEX QC Series of analyzers also allows for report of elemental and oxide concentrations as well, provided element and oxide assay values are available for the set of calibration standards.

Applied Rigaku Technologies, Inc. • 9825 Spectrum Drive, Bldg. 4, Suite 475 • Austin, TX 78717 USA
www.RigakuEDXRF.com • info@RigakuEDXRF.com • (+1) 512-225-1796

Rigaku

X-ray Diffraction Analysis for Thin Film Samples

Training Textbook

Click below to see previously published sections

4.3 Principles of X-ray Reflectivity Method

Here, for scattering with equal angles such as specular scattering, the scattering vectors are expressed as follows:

$$q_{n-1} = 2kf_{n-1} = \frac{4\pi}{\lambda} f_{n-1} \qquad \textit{Formula 4.3.23}$$

We can calculate specular reflectivity with Formula 4.3.20 by substituting the correction of Formula 4.3.22 for the Fresnel coefficient. The specular reflectivity of a uniform system without a layered structure is calculated using the following formula, instead of Formula 4.3.6:

$$R(\theta) = \frac{(\theta - A)^2 + B^2}{(\theta + A)^2 + B^2} \exp\left(-\frac{16\pi^2}{\lambda^2}\sigma^2\theta A\right) \qquad \textit{Formula 4.3.24}$$

Reference: Névot, L., Croce, P.: Revue de Physique appliquée, **15**, 761 (1980).

4.4 Reflectivity Analysis Method

Reflectivity can be analyzed by the three following methods:

1. Method giving film thickness based on the incident angle dependence of the oscillation period.
2. Method giving film thickness via the **Fourier transformation**.
3. Method giving film thickness, density, and surface or interface roughness by fitting.

Methods 2 and 3 are practical under most conditions. Reflectivity analysis generally involves one of these two methods.

4.4.1 Obtaining Film Thickness Based on the Incident Angle Dependence of the Oscillation Period

This method can only be applied to a single layer film on a substrate. While the reflectivity profile from a single layer film shows a simple oscillation, the peak positions of the oscillation are more contracted at lower incident angles. This is because the effects of refraction are more pronounced at lower angles of X-ray incidence.

The relationship between film thickness d and angular position θ_m of the m-th order peak is given by the following formulas:

1. When the δ value (δ_f) of the film is greater than the δ value (δ_s) of the substrate

$$\theta_m^2 \approx \sin^2\theta_m = \left(\frac{\lambda}{2d}\right)^2 \left(m + \frac{1}{2}\right)^2 + 2\delta_f \qquad \textit{Formula 4.4.1}$$

$$m = 0,1,2,3,...$$

2. When the δ value (δ_l) of the film is less than the δ value (δ_s) of the substrate

$$\theta_m^2 \approx \sin^2\theta_m = \left(\frac{\lambda}{2d}\right)^2 m^2 + 2\delta_l \qquad \textit{Formula 4.4.2}$$

$$m = 0,1,2,3,...$$

These formulas are solvable if we can obtain the two peaks θ_{m1} and θ_{m2} corresponding to the orders m_1 and m_2 of two oscillations. Thus, d and δ_l are given by the following formulas:

$$d = \frac{\lambda}{2}\sqrt{\frac{m_2^2 - m_1^2}{\theta_{m2}^2 - \theta_{m1}^2}} \qquad \textit{Formula 4.4.3}$$

$$\delta_l = \frac{1}{2}\frac{\theta_{m1}^2 m_2^2 - \theta_{m2}^2 m_1^2}{m_2^2 - m_1^2} \qquad \textit{Formula 4.4.4}$$

If we plot the square of the incident angle versus the square of order m, as shown in Fig. 4.4.1, the peak value can be approximated by a line. The extrapolated value gives $2d$ (= θ_c^2), and the gradient of the line gives film thickness.

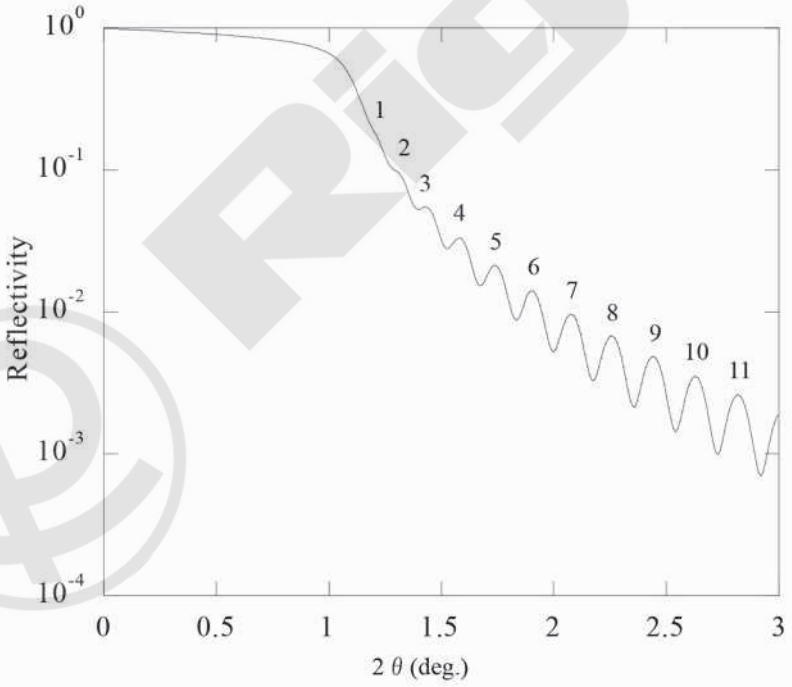

4.4 Reflectivity Analysis Method

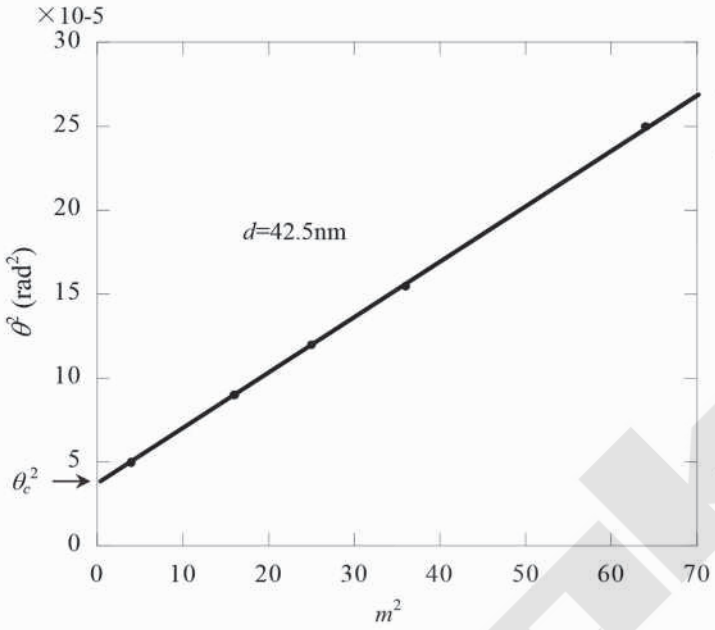

The following relationship holds between the oscillation pattern, peak position, θ_m, and film thickness d:

$$\theta_m^2 = \left(\frac{m\lambda}{2d}\right)^2 + 2\delta$$

$$= \left(\frac{m\lambda}{2d}\right)^2 + \theta_c^2$$

Here, m is the order of the peak, λ the wavelength of the X-rays, and θ_c is the critical angle.

Figure 4.4.1. Determining the thickness of a single-layer film

4.4.2 Obtaining Film Thickness via Fourier Transformation

The Fourier transformation of the oscillating components extracted from the reflectivity profile makes it possible to estimate film thickness. The procedure is given below.

1. From the measured reflectivity profile, determine a polynomial-based curve as the baseline, as shown in Figure 3.4.2. Subtract the baseline from the data and normalize the result to extract the oscillation.
2. Perform data angle correction with refractive index (δ value) of the film and obtain the oscillating components without contraction.
3. Then, apply a Fourier transform to the data and estimate thickness from the oscillating components.

Apply the results to the method based on the theoretical calculation given in the next section for efficient analysis.

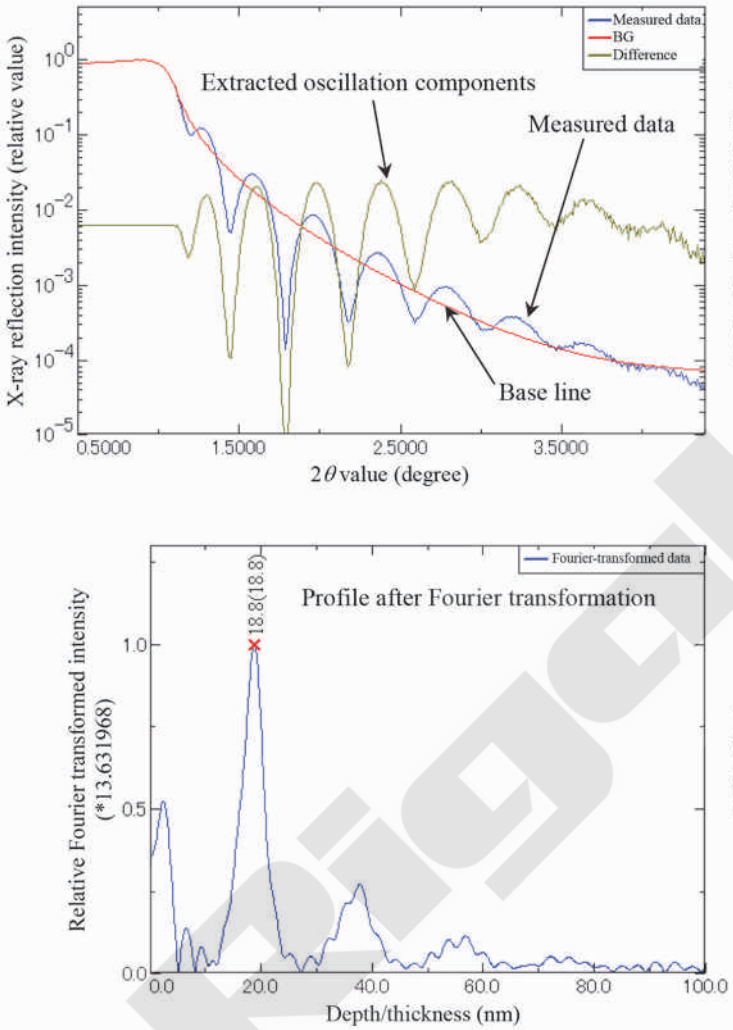

The oscillating components are extracted by subtracting the average reflectivity (baseline) from the measured reflectivity and normalizing the result.

The oscillating components are further processed by angle correction with the refractive index and by Fourier transformation.

The oscillation period gives film thickness. The results obtained are used in simulation calculations for efficient analysis.

Figure 4.4.2. Fourier transformation method

4.4.3 Obtaining Film Thickness, Density, and Surface or Interface Roughness by Fitting

A reflectivity profile including oscillation sensitively reflects the film structure. A non-linear least mean square fitting of a profile with a profile given by theoretical calculations based on a film model makes it possible to evaluate film thickness and density, as well as surface or interface roughness.

The simulation is based on the recurrence formula formulated by Parratt, as shown by Formula 4.3.20 in Section 3.3.2, combined with the surface or interface roughness described in Formula 4.3.22 in Section 3.3.3. Thus, reflectivity I/I_0 is given by $\left|R_{1,2}\right|^2$ (Formula 4.3.21).

The roughness is handled by approximating the change in average electron density at the interface between the (n-1)'-th and n-th layers as a Gaussian function and by correcting the Fresnel coefficient as in Formula 4.3.22. Roughness is expressed as root mean square (rms) roughness, σ_{n-1}.

CSDA

Crystallite Size Distribution Analysis Software

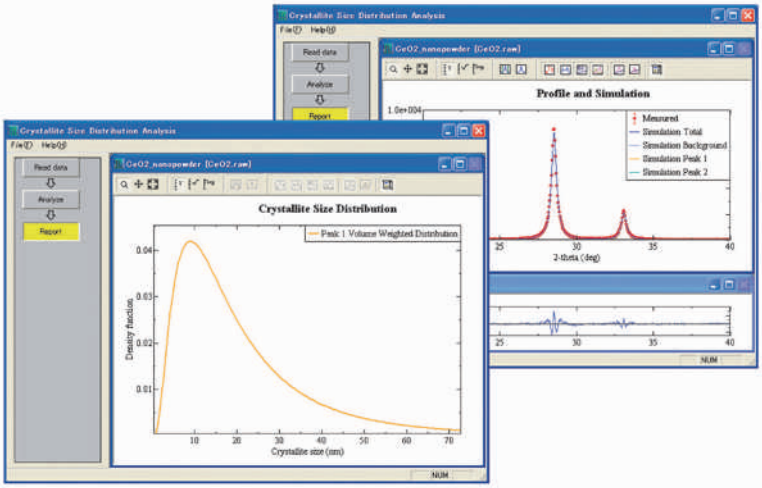

1. Introduction

Rigaku is pleased to announce the release of CSDA, a powerful new tool for determining average crystallite size and size distribution.

It is well known that the physical and chemical properties of nanoparticles change remarkably with variations in particle size. For this reason, methods for determining particle size are important for investigating the correlation between the particle sizes of a nanomaterial and its properties. It is frequently difficult to synthesize particles of uniform size, so it becomes necessary to evaluate not only the average size, but also the size distribution.

A "crystallite" is a small region of a solid which can be considered a single crystal, and in general, a "particle" is composed of one or more crystallites. Therefore, "crystallite size" is normally smaller than "particle size". The simplest method for calculating crystallite size is the Scherrer method, in which crystallite size is calculated from the width of an X-ray diffraction peak. However, the average size obtained using the Scherrer equation can be misleading, particularly when the crystallite size distribution of a sample is broad and asymmetric. CSDA overcomes this limitation by simultaneously analyzing both the width and the overall shape of a peak.

2. Advantages

2.1. Analyze size distribution from one peak

When the crystallite sizes in a sample are small, the diffraction peak width is broadened. The shape of the diffraction peak changes depending on the crystallite size distribution.

When the crystallite size distribution is narrow, the peak shape becomes roughly Gaussian—the top of the peak becomes more rounded. Conversely, when the crystallite size distribution is wide, the peak shape becomes sharp, nearly Lorentzian. CSDA can be used to determine the crystallite size and distribution of a sample by analyzing the width and peak shape of one or more X-ray diffraction peaks.

2.2. No need to measure a reference material

The shape of an experimental diffraction peak cannot be used directly to determine the crystallite size distribution. First, it is necessary to make corrections for instrumental broadening, because the peak shape

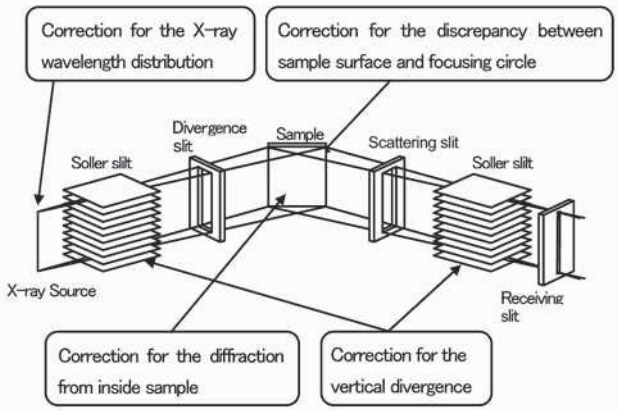

Fig. 1. Illustration of Bragg-Brentano geometry and the corresponding X-ray diffraction peak profile corrections made by CSDA.

changes depending on the experimental conditions (slit widths, specimen transparency, etc.).

CSDA automatically performs the necessary instrumental broadening corrections based on the slit width used in the measurement, the Bragg-Brentano geometry, the linear absorption coefficient of the sample etc. Because the changes in peak shape are taken into account, CSDA can calculate crystallite size distribution accurately. This also makes it unnecessary to use a standard sample to correct the diffraction peak width.

2.3. Use a conventional diffractometer

Because the profiles analyzed by CSDA are measured using the most common Bragg-Brentano geometry, neither a special diffractometer nor an attachment is necessary.

3. Application of ZnO nanocrystals

ZnO has attracted much attention because its photocatalytic properties give it potential to be used in applications for environmental sustainability. Bulk ZnO has a band gap of 3.37 eV, however, it responds to visible light and has attractive photocatalytic properties after a specific heat-treatment is applied. This is considered to be strongly related to its characteristic surface texture and crystallite sizes. Results of the determination of the average size and size distribution of heat-treated ZnO nanocrystals are described below.

Figure 2 shows the (110) X-ray diffraction peaks for ZnO heat-treated at 100 degree intervals from 400 to 800°C. It can be seen that the peaks become sharper as the treatment temperature increases, and therefore, that crystallite size increases with treatment temperature.

The measured peak profiles were analyzed by CSDA.

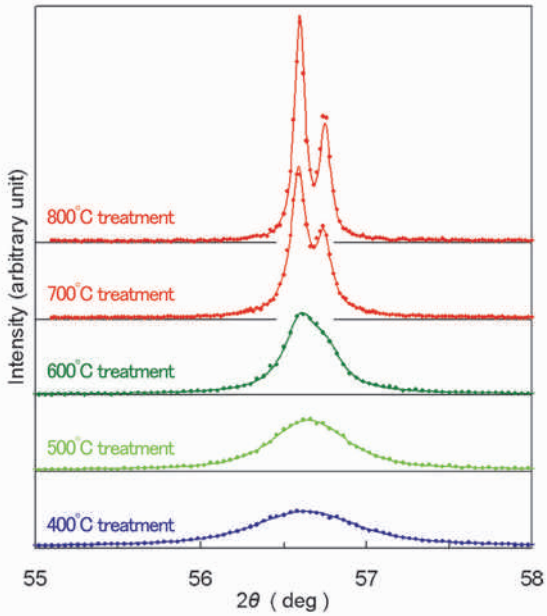

Fig. 2. ZnO (110) diffraction profiles after heat treatments; dots are measured profiles and solid lines are calculated profiles.

The number-weighted and the volume-weighted crystallite size distributions are plotted in Fig. 3, in Images A and B, respectively. Results on the average diameters of the ZnO crystallites are also shown at the top right hand corners of Images A and B.

Both the number-weighted and volume-weighted crystallite-size distributions curves become broader with increasing temperature. As expected, the average diameters of the crystallites also increase with temperature.

Samples offered by:
Prof. K. Haga, Sendai National College of Technology
Prof. T. Shishido, Institute for Materials Research, Tohoku University

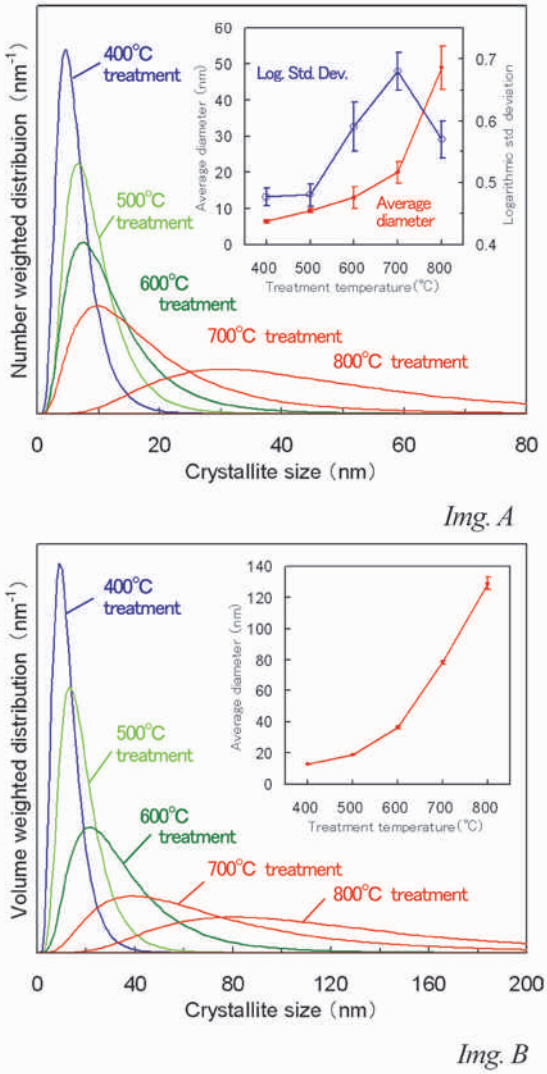

Fig. 3. Change of crystallite size distribution in ZnO nanocrystal by treatment temperature.

Img. A: Change of number weighted distribution, number weighted average diameters and logarithmic standard deviation.

Img. B: Change of volume weighted distribution and volume weighted average diameter.

Rigaku

THE BRIDGE

MATERIALS ANALYSIS eNEWSLETTER
JUNE 2014, ISSUE 12